ADVANCED SUSTAINABLE SYSTEMS
www.advsustainsys.com

A Prototypical Conjugated Polymer Regulating Signaling in Plants

Gabriele Tullii, Federico Gobbo, Alex Costa, and Maria Rosa Antognazza**

The use of nanomaterials has been very recently introduced in plant biotechnologies, for both the monitoring and the enhancement of plants functions. Several functional interfaces between living plants and nanotechnology have been successfully reported for diverse applications, from sensing to photosynthesis and energy production and from modulation of physiological activity to controlled delivery of chemicals. In this work, a photoactive, biohybrid interface based on a prototypical semiconducting polymer, sensitive to green light, and *Arabidopsis thaliana* plants is reported. Optical excitation of polymer beads is shown to deterministically regulate the *Arabidopsis* stomatal aperture, the leaf pores which regulate the plant carbon dioxide uptake, oxygen release, and transpiration processes. Moreover, it is observed that excitation of bio-polymer hybrid interfaces optically modulates the cytosolic calcium ions concentration, which is involved, as a second messenger, in the regulation of stomatal movements. The results support the possibility to employ light-responsive organic materials to regulate on demand the physiological activity of plant systems, in a drug-free, touchless, and easily controllable way. When transferred to the field, this strategy may represent an innovative approach to optimize the exchange of gases and water loss of plants, and to improve the plant resilience toward environmental constraints.

1. Introduction

The central role that plants play both in the ecosystem, as regulators of water cycles and atmospheric oxygen, and in human life as a source of food, chemicals, heat, and materials, aimed researchers to find solutions to increase plant growth and functions, especially in constrained conditions.[1] Up to date, the approaches employed to this purpose are mainly based on increased input of resources (fertilizers, agrochemicals, and water through irrigation), often linked to environmental risks, and on plants genetic improvement.

In this scenario, smart materials and devices have been only recently introduced for both the monitoring and the enhancement of plants functions. The field of "plant nanobionics," as defined in a recent review by M. Strano et al., has been rapidly emerging in the past 5 years, and several innovative applications can be envisioned, from sensing to energy generation, from plant-based innovative materials to actuators.[2,3] Examples of functional nanomaterials reported so far include organic and inorganic nanoparticles (NPs),[4,5] carbon nanotubes,[6] carbon dots,[7] and metal–organic frameworks.[8] In some cases, noticeable modulation of plant physiological activity was observed, with effects on root elongation, seed germination, plant growth, enhancement of the photosynthesis process, and reduction in water consumption.[9,10] The M. Berggren's and E. Stavrinidou's research group pioneered the realization of smart interfaces between devices based on organic conductors and plant systems, introducing the concept of electronic plants.[11] Interestingly, they reported the fabrication of hydrogel-like conducting wires, embedded within the plant vascular tissues, using water soluble thiophene-based polymers and oligomers, respectively, self-organized and in situ polymerized inside *Rosa floribunda* plants.[11,12] Moreover, they exploited the plant-integrated electronic systems for the in vivo manufacturing of organic electronic analog and digital circuits, encompassing organic electrochemical transistors (OECT) and supercapacitors devices based on the self-doped electrically conducting polymer poly(3,4-ethylenedioxythiophene) (PEDOT-S:H).[11–13] Textile-based OECTs integrated into the plant structure were also reported to efficiently record plant physiological parameters,[14] opening the way to the implementation of "organic bioristors" for real-time and dynamical monitoring of the

G. Tullii, F. Gobbo, M. R. Antognazza
Center for Nano Science and Technology@PoliMi
Istituto Italiano di Tecnologia
via Pascoli 70/3, Milan 20133, Italy
E-mail: mariarosa.antognazza@iit.it
F. Gobbo
Department of Physics
Politecnico di Milano
P.zza L. Da Vinci 32, Milan 20133, Italy
A. Costa
University of Milan
Department of Biosciences
Via G. Celoria 26, Milan 20133, Italy
E-mail: alex.costa@unimi.it
A. Costa
Consiglio Nazionale delle Ricerche
Institute of Biophysics
Via G. Celoria 26, Milan 20133, Italy
The ORCID identification number(s) for the author(s) of this article can be found under https://doi.org/10.1002/adsu.202100048.

DOI: 10.1002/adsu.202100048

changes in the plant sap following vapor pressure deficit, and, in perspective, for a more efficient and sustainable use of water resources.[15] In this scenario, semiconducting conjugated polymers, endowed with intrinsic responsivity to visible light and opto–electronic properties, represent optimal candidates for the development of optically sensitive interfaces with plant systems. Surprisingly, they were very rarely considered, for applications restricted to imaging[16] and photosynthesis enhancement.[10]

Herein, we investigate the effect of polymer photoexcitation on plant signaling, with the purpose to develop a proof-of-concept functional interface between a synthetic material sensitive to visible light and a plant system. We chose *Arabidopsis thaliana* (*A. thaliana*) as a widespread plant model, widely accepted in a variety of different studies, including plant physiology, population genetics, evolution, and environmental science.[17,18] We realize hybrid interfaces between a prototypical conjugated polymer, namely region-regular poly(3-hexylthiophene-2,5-diyl) (P3HT), either in the form of thin solid film or of micrometer-sized beads dispersed in water, and *A. thaliana* guard cells (GCs). GCs are highly specialized, kidney-shaped cells, which juxtapose to form a pore, the stoma. Importantly, they contain photosynthetically active chloroplasts, and their volume variations, as the macroscopic result of a complex network of molecular processes at different hierarchical scales,[19] govern stomatal movement. Thus, GCs play a key-role in carbon dioxide uptake from the environment, oxygen release, transpiration processes, and they ultimately rule plant growth and survival.[19]

In this paper, we demonstrate that P3HT optical excitation deterministically leads to a significant modulation of the stomatal aperture size. We also monitor the variation on intracellular calcium ions (Ca^{2+}) concentration, induced by the treatment with the P3HT beads and green light excitation, by employing *A. thaliana* plants expressing the genetically encoded Ca^{2+} indicator yellow Cameleon 3.6 localized in the cytosol (NES-YC3.6).[20] Ca^{2+} signaling participates in many regulatory processes as a second messenger.[21] A plethora of environmental and developmental stimuli determine an increase of cytosolic Ca^{2+} concentration ($[Ca^{2+}]_{cyt}$).[22,23] In particular, in plant cells cytosolic Ca^{2+} oscillations regulate different processes such as pollen and root hair growth, as well as stomatal closure induced by the wounding-associated hormone jasmonic acid and the drought hormone abscisic acid (ABA).[24–26] Interestingly, we observe that optical excitation of P3HT/GC biohybrid interfaces determines the reversible modulation of cytosolic Ca^{2+} concentration, with no detrimental effects on GC physiological functions.

This work represents a proof-of-concept of a functional, optically activated interface between a semiconducting conjugated polymer and a plant system. In particular, the opportunity to finely regulate the opening and closing state of stomata could help to increase plant resistance to drought stress and to optimize plant water adsorption. In perspective, the capability to trigger and control on-demand, with high spatial and temporal resolution and in a minimally invasive manner, specific functionalities of plant systems by using solar light may open the path to the development of innovative solutions in the field of plant photobionics.

2. Results and Discussion

2.1. Polymer Nanoparticles/Guard Cells Interface: Realization, Biocompatibility, Nanoparticles Localization

We realize a biohybrid interface between a prototypical conjugated polymer, namely region-regular P3HT and leaf epidermal cells isolated from *A. thaliana*, a widely accepted plant model system (**Figure 1**).

Several reports from our and other groups have reported functional, optically active interfaces between P3HT-based devices and animal systems.[27–35] In particular, previous works demonstrated the P3HT optimal biocompatibility,[36] its longer-term photochemical and stability properties in water and in physiological conditions,[37] electronic and electrochemical behavior upon photoexcitation in an ionic environment,[28,38,39] and, most importantly, the capability to optically modulate different, physiologically relevant processes in mammal cells.[29,30,40,41] To promote the realization of interfaces with biological systems, P3HT beads have been also realized with different methods[42,43] and successfully employed as artificial photoactuators in pigs.[44] Based on the extensive characterization and excellent performance of P3HT-based materials and devices with animal models, we selected this same material as a benchmark to realize an optically addressable, functional interface with plant cells. We realize interfaces with plant cells by employing P3HT both in the form of thin films and in the form of NPs. P3HT NPs' synthesis and characterization has been reported elsewhere,[42] and briefly summarized here in the Experimental Section. Figure 1a shows the P3HT optical absorption spectrum in both configurations. P3HT NPs spectrum shows a red-shift of ≈35 nm, possibly caused by highly stacked and closely packed chains in the aggregate state induced within the water dispersion.[42] The P3HT chemical structure is also shown in Figure 1a, inset. Importantly, P3HT optical absorption spectrum, peaking in the green, does not substantially overlap with the absorption spectra of UV-B, blue and far-red plant photoreceptors (i.e, UVR-8, cryptochromes, phototropins, and the Pfr form of phytochrome), and only partially with the Pr form of phytochrome,[45] thus limiting the need to disentangle effects of endogenous plant light sensitivity from polymer photoexcitation. Figure 1b shows a representative scanning electron microscopy (SEM) image of a P3HT NP belonging to the NPs dispersion used in this study. As previously reported,[29] typical NPs dimensions are in the order of 240 ± 80 nm.

As for the biological counterpart of the hybrid interface, we focus on stomata GCs in isolated leaf epidermis from *A. thaliana* mature plants.[46] GCs are a particularly interesting target for our study, since they are present in the leaves, they can be accessible in a relatively easy way and, most importantly, they have key roles in the plant development, as well as in the response to external stimuli and in metabolic and respiratory processes. GCs show a kidney-shaped morphology, and two cells juxtapose to form the stoma (Figure 1c). It is possible to get an easy access to GC from the other cell layers and component in *Arabidopsis* leaves by using a fast and simple procedure known as epidermal strip.[46] The subsequent steps are schematically represented in Figure 1d. Briefly, 6-week-old *Arabidopsis* leaves are attached to glass slides and the upper epidermal cells are removed by using a razor blade. The

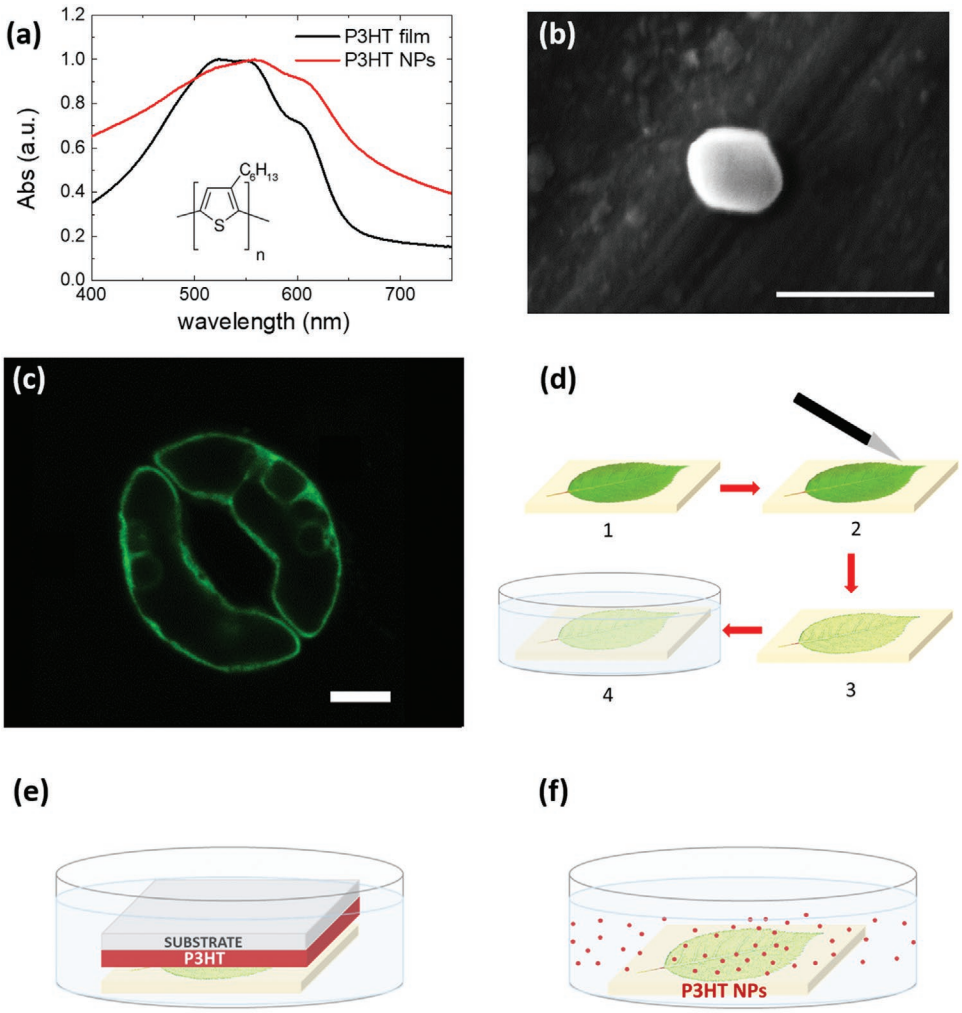

Figure 1. P3HT/guard cells hybrid plant/polymer interfaces. a) Optical absorption spectrum of P3HT thin films and NPs. The inset depicts the P3HT chemical structure. b) Representative SEM image of a single P3HT NP. Scale bar: 500 nm. c) Representative fluorescence image of GCs expressing the NES-YC3.6 Cameleon sensor. Scale bar: 5 µm. d) Schematic drawing of the main steps for epidermal strip. e,f) Cartoon depicting hybrid plant/polymer interfaces realized by placing GCs directly in contact with P3HT thin films and P3HT NPs.

exposed GCs are then placed in a proper imaging solution. Finally, the realization of the hybrid plant/polymer interface is completed either by putting in contact the GC onto the glass slide with the polymer thin film (Figure 1e), or by delivering the NP water dispersion to the cells bath (Figure 1f).

To the best of our knowledge, this is the first report of use of P3HT conjugated polymer in combination with a plant system. Thus, cell viability upon contact with the synthetic photoactive material, in dark conditions and upon photoexcitation, needs to be primarily assessed (**Figure 2**). A viability study based on fluorescein-diacetate (FDA) assay was carried out. FDA, a consolidated probe for the study of both animal and plant cells viability,[47,48] is a non-fluorescent compound that switches to the fluorescein fluorescent form when hydrolyzed by the intracellular esterase of cells preserving intact membranes and regular enzymatic activities. Thus, only healthy cells become fluorescent. Figure 2 shows representative bright-field optical microscope images (panels Figure 2a,c,e) and FDA fluorescence staining over the same field of view (panels Figure 2b,d,f). The comparison with bright-field conditions allows distinguishing between viable and not-viable cells. The experiment has been carried out in dark, upon continuous wave light excitation (λ = 540 nm, 64 mW mm^{-2}, time duration = 2 min) and in the presence of the P3HT interface. The statistical analysis is done by considering 50 cells belonging to three statistically independent samples for each condition and it is summarized in Figure 2g. No statistically significant differences are evidenced among the three samples cohorts; the percentage of healthy cells being 72 ± 6%, 81 ± 8%, and 74 ± 13% in the case of control in dark, light treated, and light + polymer samples, respectively (Student's *t*-test, $p > 0.05$ in all considered cases).

The capability of P3HT NPs to cross the cytosol membrane and to internalize within living cells is dependent on the considered biological model; in fact, previous reports have shown that they rapidly internalize within HEK-293 line cells,[29,42] but not within hippocampal neurons.[44] Moreover, the impact of the zeta-potential and the hydrodynamic size of different nanomaterials on the interaction with leaf cell surfaces has been rarely addressed in a systematic way.[49] Recent works investigated a few nanomaterials, both organic[4] and inorganic (carbon dots, cerium

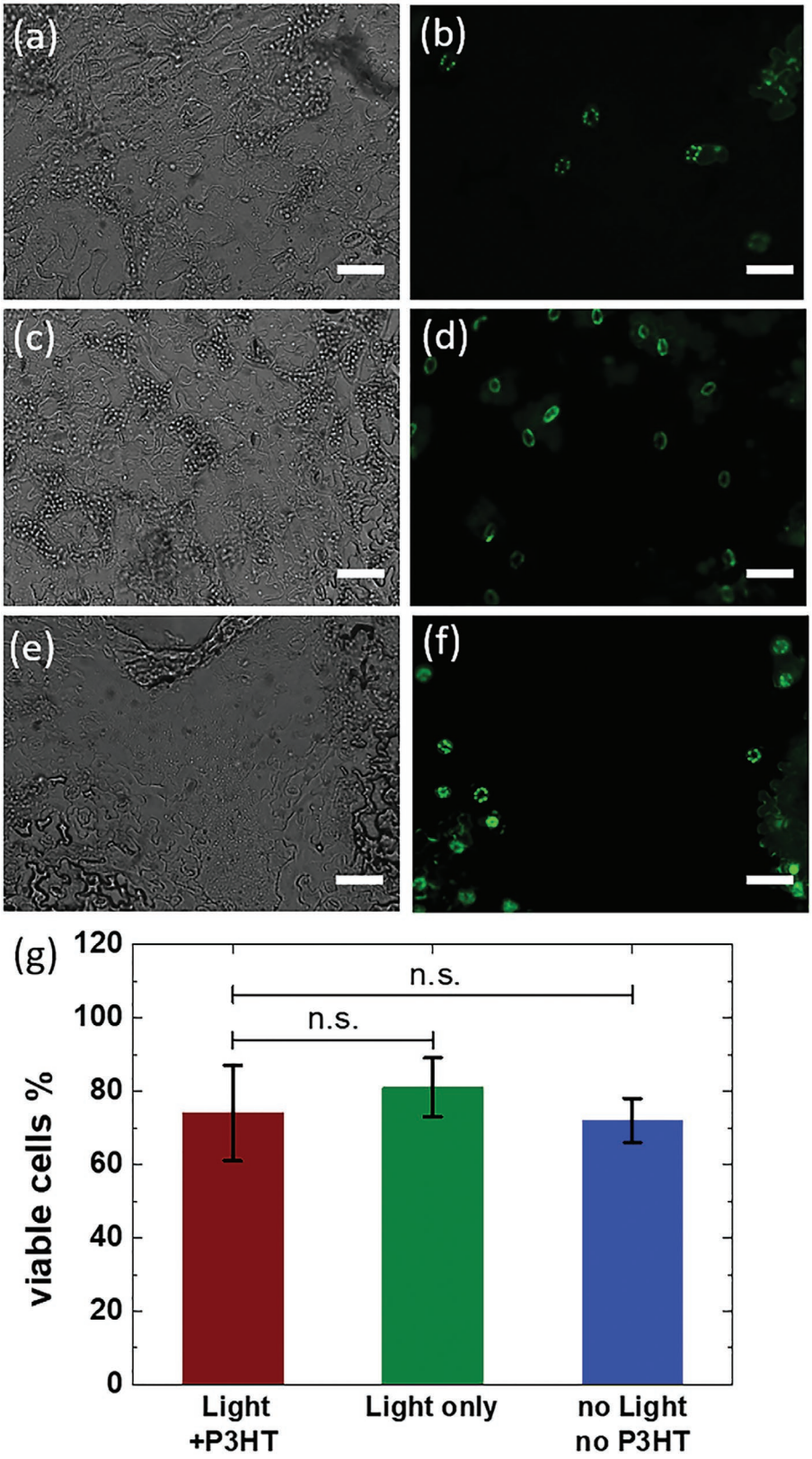

Figure 2. Guard cells viability assay. Representative bright field and FDA fluorescence emission of guard cells a,b) without any treatment, c,d) after green light excitation, and e,f) after green light excitation in presence of P3HT. Light stimulation conditions: $\lambda = 540$ nm, 64 mW mm^{-2}, time duration = 2 min. Scale bars: 50 µm. g) Percentage of viable cells for each condition. No statistically relevant difference among the three samples cohorts is evidenced (Student's *t*-test, $p > 0.05$ in all considered cases).

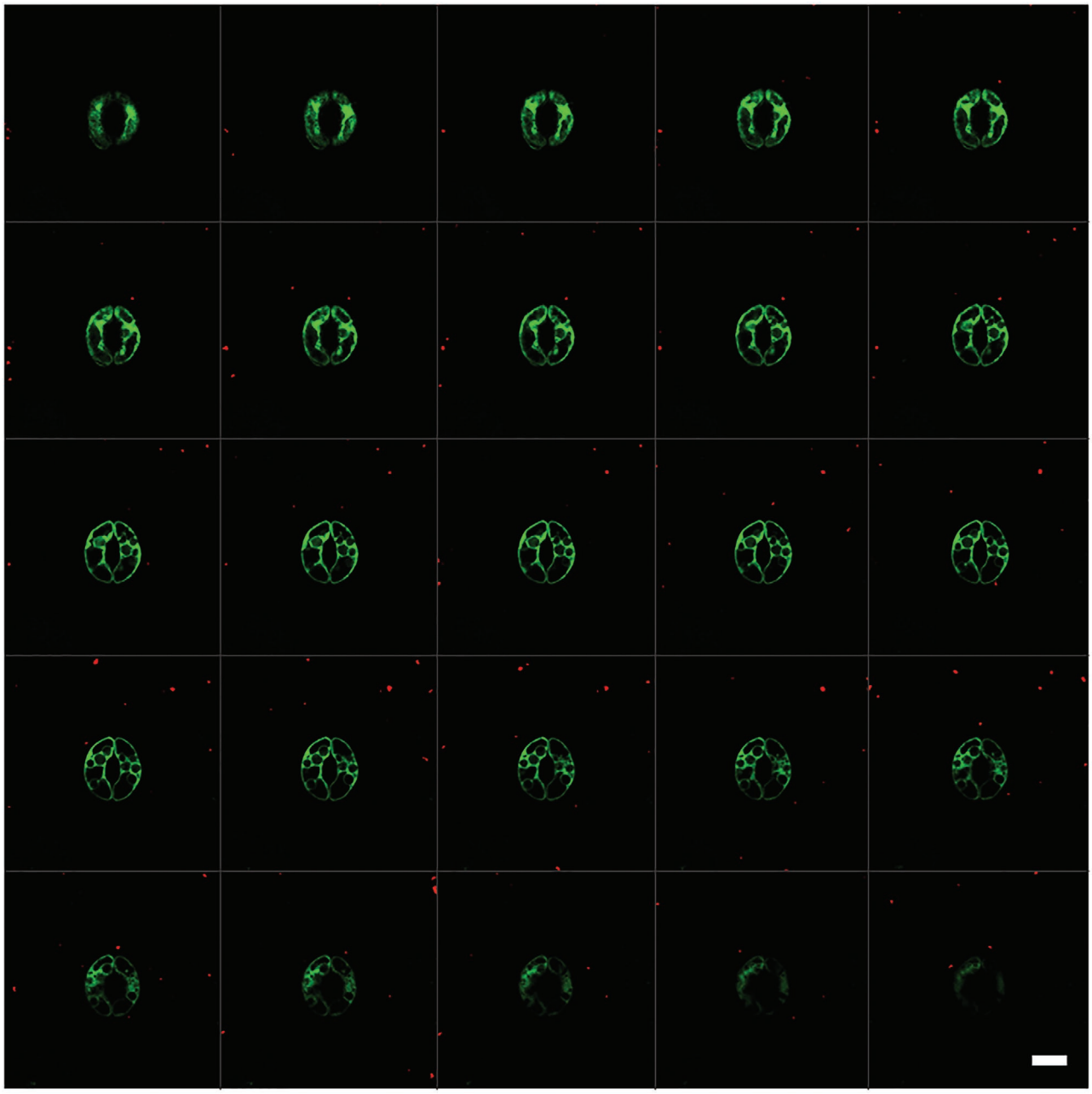

Figure 3. NPs confocal imaging. Confocal optical sections depicting an *Arabidopsis* GC treated with rr-P3HT NPs (OD value 0.1, incubated for 20 min prior to image acquisition). *Arabidopsis* GCs are stained with YC3.6 (green). P3HT NPs are visualized through their intrinsic emission (red). Scale bar: 10 µm. At all considered focal planes, from the bottom glass interface (upper left image) to the top interface with the extracellular bath (lower right image) NPs do not cross the GC membrane.

dioxide, and silicon dioxide).[49] Thus, we employ confocal fluorescence microscopy to check the capability of P3HT NPs to internalize within GC. **Figure 3** shows confocal optical sectioning, from the bottom interface with glass toward the top interface with the culture bath, of a representative GC from plants expressing the NES-YC3.6 Cameleon sensor[20] (green fluorescence in Figure 3) exposed to P3HT NPs (NPs optical density [OD] = 0.1; steps between adjacent planes, 250 nm). The optical emission properties of P3HT NPs in the red region of the visible spectrum allow their direct localization, thus avoiding the need to stain with fluorophores, which may eventually alter their internalization dynamics. Data show that NPs are not internalized within the GCs cytosol, and remain suspended in the extracellular bath solution, possibly due to NPs hydrophobicity and size.

2.2. Polymer Nanoparticles Optically Control Stomata Aperture State and Ca^{2+} Signaling

GC are primarily involved in the modulation of CO_2 uptake, O_2, and transpiration, which de facto are fundamental to regulate plant growth and productivity.[50] Thus, they do represent

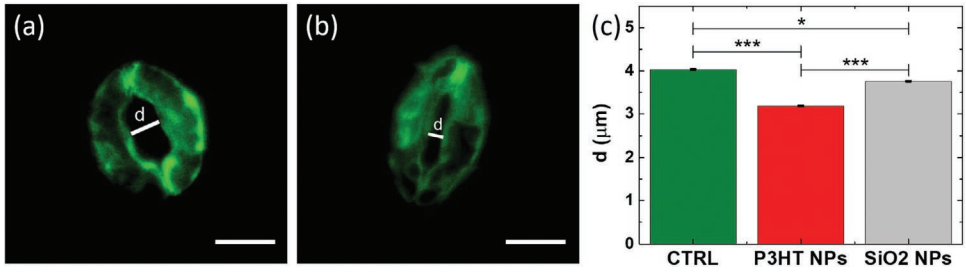

Figure 4. Stomata aperture variation upon white light illumination. Representative fluorescence images of GCs expressing the NES-YC3.6 in a) open and b) closed states. Scale bars: 10 μm. c) Histogram reporting the average stomatal aperture width (*d*) measured after exposure to white light in absence of NPs (CTRL), and in presence of rr-P3HT or optically inert SiO_2 NPs. Error bars represent the standard error of the mean, s.e.m. $*p < 0.05$, $***p < 0.001$ (Student's *t*-test).

an ideal, target system for the development of a functional, optically driven interface between P3HT NPs and plant cells. To this purpose, we investigate the occurrence of a macroscopic variation in the average stomatal aperture, possibly induced by photoexcited P3HT NPs (**Figure 4**). We carry out widefield fluorescence microscopy imaging experiments in GC populations, of plants expressing the genetically encoded NES-YC3.6 Calcium sensor, either untreated or treated with P3HT NPs. It is known that exposure of GC to visible light, and in particular to blue and red wavelengths, provokes stomatal opening.[51] Thus, we preliminarily expose GCs to white light (light intensity 4000 lux, matching conditions of sunlight illumination in a cloudy day) for 90 min. This treatment absolves a double function: it serves both as a photoexcitation for the NPs, since the maximum P3HT NPs responsiveness falls in the green region of the visible spectrum (Figure 1a), and at the same time as a stimulus for provoking stomatal aperture in environmentally significant conditions. In this way, by measuring the stomatal pore size it is possible to evaluate the influence of the NPs on the light-induced stomatal aperture. Figure 4 shows representative fluorescence images of GCs in open and closed states (panels Figures 4a,b, respectively); the average stomatal aperture width, *d,* defined as the minor semi-axis of the geometrical ellipse defined by the stomatal aperture, is also schematically indicated. Figure 4c shows *d*-mean values immediately after the optical treatment, in both untreated and NP-treated GC. In order to discriminate a possible effect of the NPs steric hindrance from the effect of light excitation, we also employ optically inert silica NPs (SiO_2 NPs, average diameter = 260 ± 10 nm, concentration = 0.25 mg mL^{-1}), of proven biocompatibility,[49] as negative controls. The data reveal a significant decrease in stomatal aperture in the case of P3HT NPs in comparison to the untreated samples (CTRL), with a significant variation of more than 20%. The control, optically insensitive SiO_2 NPs shows also a decrease in the average stomata aperture, with a variation of ≈7% as compared to untreated samples, suggesting that the presence of NPs intrinsically leads to a partial inhibition of the light-induced stomatal aperture. Interestingly, a similar result was obtained with CuO NPs; in this case, the contact between the NPs and the GCs stimulated the stomatal closure through a process regulated by the intracellular production of hydrogen peroxide (H_2O_2).[5]

However, the most striking variation in stomatal aperture can be ascribed to P3HT NPs' photoexcitation. Importantly, we observe that light excitation, mediated by NPs optical absorption, deterministically leads to a partial inhibition of the stomatal aperture, thus possibly resulting in functional modulation of plants physiological activity and on-demand control of responses to external stimuli, like humidity, CO_2 concentration, and sunlight intensity. As an example, this approach could be used to reduce or modulate the speed of stomatal aperture to prevent an excessive water loss in hot days, thus preventing the possible wilting of the plant, while allowing a proper CO_2 provision.[52]

The identification of the underlying mechanism would be key to gain fine, quantitative, and on-demand modulation of stomatal aperture, possibly adapting to different stimuli and environmental conditions. Though, this is not a trivial task, mainly because even the intrinsic physiological mechanisms, active at the single cell levels, are still currently under intensive investigation and have not been completely clarified, due to the close entanglement of stimuli of different origin leading to stomatal closure and/or to stomatal aperture inhibition.[53] In brief, literature reports demonstrated that the inhibition of the stomatal opening can be obtained through several, possibly intertwined mechanisms, including i) administration of hormone ABA;[54,55] ii) mechanical stimulation;[56] iii) cold thermal shock;[57] iv) generation of reactive oxygen species (ROS), mainly H_2O_2;[58] and v) increase of extracellular Ca^{2+}.[55,59] Interestingly to this work, the addition of exogenous H_2O_2 has been shown to inhibit the stomatal opening provoked by excitation with blue and red wavelengths in *A. thaliana* plants.[60] The overall picture is further complicated by the mutual interplay existing between Ca^{2+} ions signaling and ROS/NOS species, at physiological or toxic concentrations, currently object of intensive studies.[61–64]

In the attempt to identify the most plausible modulation process leading, upon P3HT NPs light excitation, to inhibition of stomatal aperture, we can safely disregard mechanisms (i) to (iii), since: a) we do not administer any chemical compound; b) control measurements with SiO_2 NPs, with dimensions comparable to P3HT NPs, demonstrate that the steric hindrance due to the sole presence of exogenous beads has a limited effect on stomatal diameter change, while photoexcitation of light sensitive NPs plays a significant major role in the observed phenomenon; c) we do not induce temperature decrease in the cell bath (conversely, photoexcitation may in principle lead to a localized heating effect, but in any case the thermal shock is expected to be completely negligible in the

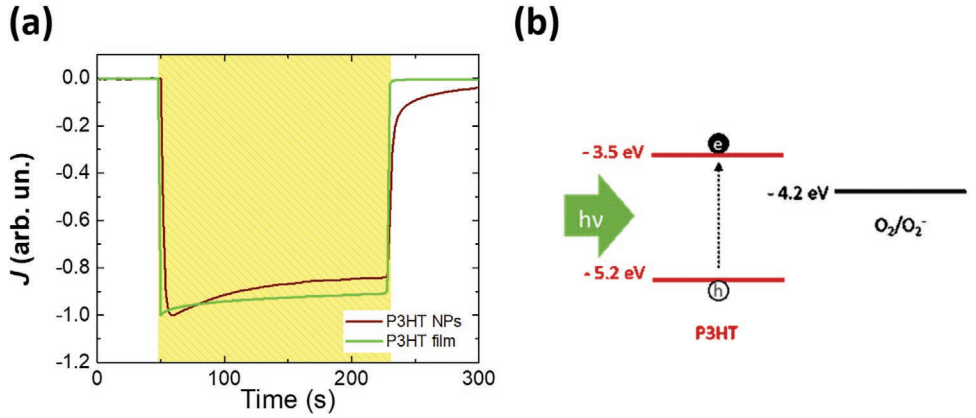

Figure 5. Photocathodic current generation by P3HT NPs dispersion. a) Comparison among photocurrent (*J*) signals (normalized to the maximum absolute *J* values) obtained in P3HT NPs dispersion and P3HT thin films spin-coated from solution onto the ITO slab. Photoexcitation is represented by the yellow-shaded area (LED emission wavelength peak, 470 nm; stimuli duration, 3 min; photoexcitation density, 2.7 mW mm^{-2}). b) P3HT HOMO/LUMO energetic levels are compatible with oxygen reduction reactions occurring at the polymer/electrolyte interface.

case of NPs at the working concentrations and light excitation density). Thus, we restricted our attention onto mechanisms (iv) and (v). We have recently demonstrated that biohybrid interfaces between P3HT polymer and mammal cells can lead to a modulation of intracellular Ca^{2+} concentration[29,30] as well as to localized production of ROS species.[65] Thus, both mechanisms may in principle play a role in the observed change of stomatal state.

Both P3HT thin films and P3HT NPs within an aqueous environment preserve the capability to generate charges upon photoexcitation and sustain electron transfer processes at the interface.[28,29,38] It was unambiguously demonstrated that the predominant photoelectrochemical reaction at the thin film polymer surface is reversible oxygen reduction, which leads to the creation of ROS and, ultimately, to H_2O_2 production.[65] **Figure 5**a shows the comparison between photocurrent dynamics recorded by using P3HT polymer thin film, spin-coated from solution on top of an indium–tin–oxide (ITO) electrode and used as the working electrode, and P3HT NPs aqueous dispersion, in contact with an ITO electrode. Importantly, in both cases the negative photocurrent sign indicates a photocathodic mechanism, in which photogenerated electrons react with chemical species present in the electrolyte solution. Furthermore, we notice that the P3HT HOMO and LUMO energetic levels (≈5.2 and ≈3.5 eV, respectively) are well-aligned, respectively, with the underlying ITO electrode work function (≈4.5 eV) and the oxygen reduction reaction, O_2/O_2^- (≈4.2 eV), in full agreement with this picture (Figure 5b).

Figure 5 supports the production of ROS species, all virtually ending up into increased H_2O_2 concentration, as a plausible mechanism to explain the optically triggered inhibition of stomatal aperture state, observed in presence of photoexcited NPs (mechanism [iv]).

Optical modulation of GC Ca^{2+} signaling is also addressed, as another possible phototransduction mechanism (mechanism [v]) active at the interface between P3HT NPs and *A. thaliana* GCs. Literature reports demonstrated that modulation of Ca^{2+} concentration can in fact lead to sizable inhibition of stomatal aperture. More generally, oscillations in cytosolic free Ca^{2+} concentration have been proposed to encode information that overall controls stomatal closing and opening states.[26,66]

We monitor the GC spontaneous cytosol Ca^{2+} oscillations, in presence and absence of P3HT NPs, in control conditions (i.e., pulsed blue light conditions[67]) and after green light excitation (**Figure 6**). Ca^{2+} signals consist in transient increases in $[Ca^{2+}]_{cyt}$ that arise from Ca^{2+} fluxes coming from the extracellular environment or from internal compartments of the cells.[23,24] External stimuli, such as temperature changes, salt or osmotic stresses, light, and plant hormones, produce specific Ca^{2+} responses with defined spatial and temporal characteristics, called Ca^{2+} signatures.[21,68] To quantitatively monitor $[Ca^{2+}]_{cyt}$, we employ *A. thaliana* plants expressing the genetically encoded cytosol-localized calcium indicator yellow Cameleon NES-YC3.6.[17] YCs probes are based on the fluorescence resonance energy transfer (FRET). They comprise two GFP variants, cyan and yellow fluorescent proteins (CFP and YFP, respectively) bound together by the calmodulin-binding peptide M13 and the Ca^{2+}-binding protein calmodulin.[69] When Ca^{2+} ion binds to calmodulin, a conformational change in the YC indicator takes place, enabling enhanced FRET between CFP and YFP. In brief, the YC probe fluorescence emission (YFP/CFP ratio) is directly proportional to the Ca^{2+} concentration and can be quantitatively monitored by fluorescence microscopy.

Figure 6a,b displays typical spontaneous $[Ca^{2+}]_{cyt}$ oscillations observed in stomata GCs when leaves and leaf epidermal strips are immediately imaged after their detachment from the plants.[67,70,71] This piece of data is indeed in line with literature data available for *Arabidopsis* GCs.[70,72,73] Although the nature of the spontaneous $[Ca^{2+}]_{cyt}$ oscillations has not been fully elucidated yet, experiments performed on GCs of intact plants have confirmed that this spontaneous Ca^{2+} activity is a conserved feature of this cell type, and it is probably related to physiological processes taking place in response to environmental stimuli (e.g., water balance, light conditions, and CO_2 levels)[70] and to the electric potential of the plasma membrane.[74]

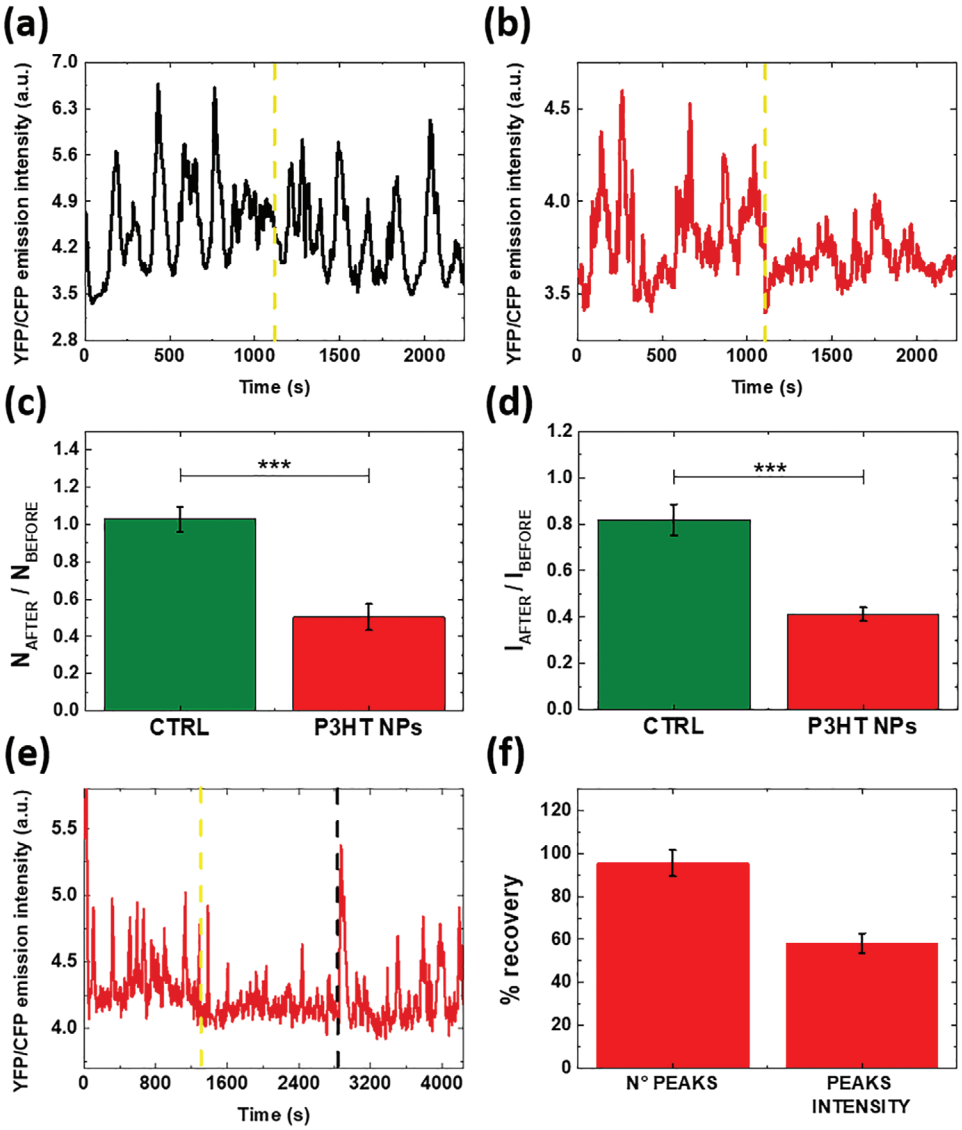

Figure 6. P3HT NPs and green light excitation reversibly modulate intracellular Ca^{2+} dynamics in *Arabidopsis thaliana* guard cells. a,b) Representative Ca^{2+} oscillations, in terms of YFP/CFP emission ratio, before and after optical excitation, in absence and presence of P3HT NPs (panels [a] and [b], respectively). The yellow dashed line represents the optical excitation (λ = 540 nm, intensity: 64 mW mm^{-2}, time duration = 2 min). c,d) Mean ratio between the average number of YFP/CFP emission peaks (c) and emission intensity (d), after and before illumination protocol. Mean values are averaged over a statistical ensemble of n = 10 cells for each condition. Error bars represent the s.e.m. ***$p < 0.001$ (Student's t-test). e,f) Reversibility of the intracellular Ca^{2+} modulation is assessed by leaving the GC sample resting in dark. The yellow and black dashed lines represent the optical excitation (λ = 540 nm, intensity: 64 mW mm^{-2}, time duration: 2 min) and the time spent in dark (20 min), respectively. (f) shows the percentage recovery of the average number and amplitude of YFP/CFP spikes after leaving the guard cells in dark. Mean values are averaged over a statistical ensemble of n = 20 cells. Error bars represent the s.e.m.

The comparable $[Ca^{2+}]_{cyt}$ dynamics recorded in control, pulsed blue light conditions (i.e., before green light excitation protocol, traces on the left of the dashed yellow line) further confirm that in absence of a green light stimulus, the GCs functional properties are not affected by the sole P3HT NPs presence.

After optical excitation, the situation changes. It has been reported that photoexcitation with blue and red wavelengths can substantially affect Ca^{2+} signaling, leading to an increase in the $[Ca^{2+}]_{cyt}$ mediated by the action of specific photoreceptors, phototropins and phytochrome for blue and red light, respectively.[21,75–78] The use of green light excitation in principle allows to exclude any effect mediated by light sensitive proteins. This assumption is fully confirmed by the results obtained with the P3HT NPs-untreated GCs (CTRL), without relevant changes neither in the $[Ca^{2+}]_{cyt}$ peaks amplitude nor in their number evaluated over the pre- and post-excitation temporal windows (Figure 6c,d, CTRL histograms). The variation is quantified by calculating the ratio between the average peaks' amplitude after and before light (I_{AFTER}/I_{BEFORE}) and the ratio

of the mean number of peaks recorded after and before the light stimulus occurrence (N_{AFTER}/N_{BEFORE}). Both quantities are very close to unity in the CTRL case ($N_{AFTER}/N_{BEFORE} = \approx 1$, $I_{AFTER}/I_{BEFORE} = \approx 0.8$). Conversely, the illumination of the P3HT NPs leads to a significant variation of Ca^{2+} dynamics. Figure 6b shows representative Ca^{2+} oscillations before and after photoexcitation. Remarkably, N_{AFTER}/N_{BEFORE} and I_{AFTER}/I_{BEFORE} values show a percentage variation of about −51% and −49% as compared to the CTRL case (Figure 6c,d). Interestingly, a similar effect can be achieved by placing a P3HT thin film directly in contact with GC and adopting the same illumination protocol (Figure S1, Supporting Information).

We evaluated the reversibility of the variation in cytosolic Ca^{2+} oscillations frequency and peak intensity by leaving the samples resting in dark for 20 min (Figure 6e,f; the dark condition is represented by the black dashed line). Histograms show that the recovery of the oscillations frequency is nearly complete (95% ± 6% recovery), while their average amplitude is only partially restored (58% ± 5% recovery). However, this latter effect can be also ascribed to partial bleaching of the probe efficiency with time. These results allow us to conclude that the optically induced variation in the GCs $[Ca^{2+}]_{cyt}$ spontaneous oscillations, mediated by P3HT NPs, is not irreversible, thus excluding the presence of detrimental consequences on GCs viability and physiological functionality.

In the literature several pieces of evidence have shown that a large variety of external stimuli, including extracellular Ca^{2+} addition, modulate the $[Ca^{2+}]_{cyt}$ in GCs, which in turn leads to the regulation of stomatal aperture/closure dynamics. The most commonly observed effect is a transient increase in GCs $[Ca^{2+}]_{cyt}$; however, in some cases, effects on the spontaneous $[Ca^{2+}]_{cyt}$ oscillations were also observed. Interestingly, specific oscillations' frequency ranges in $[Ca^{2+}]_{cyt}$ have been identified to have sizable consequences on stomatal movements, apparently even in absence of any other additional signaling component. The identification of oscillations' frequency ranges being more favorable to stomatal closure arises from a delicate balance in the membrane voltage, driving K^+, and anions efflux across the GC.[66,74] Even more, a defined range of GC Ca^{2+} oscillations parameters (frequency, transient number, duration, and amplitude) was found to encode stomatal movements, and to change steady-state stomatal aperture.[79] Overall, ideal frequency of Ca^{2+} oscillations are required to elicit maximal reduction in stomatal aperture, independently on absolute Ca^{2+} concentration increase. In other words, Ca^{2+} increase causes rapid, short term stomata closure; however, Ca^{2+} oscillation parameters are responsible for a long-term calcium programmed decrease in the steady state aperture. Following calcium reactive closure, GCs elicit programmed changes in aperture by decoding the information contained in Ca^{2+} oscillation parameters, and appropriate parameters were found to inhibit stomatal opening.

In analogy with these reports, we hypothesize that the inhibition of the stomatal aperture might be due to a favorable, reversible variation of Ca^{2+} oscillation parameters. However, currently available data cannot definitely support or negate this hypothesis. In depth investigation of GC membrane potential, as well as experiments with specific pharmacology treatments and analysis at a molecular level, are needed to clarify the actual phototransduction process and to attribute it to mechanism (iv), mechanism (v), or to a combination of the two. This study is beyond the goal of the present work and will be the object of future investigation.

Our results are promising toward the development of functional interfaces to enhance plant resistance to drought and potentially increase their water-use efficiency, as well as to regulate on demand water adsorption/dispersion by stomata. However, a critical point in this direction will be the capability to develop hybrid systems in vivo, and not only in simplified in vitro conditions like the ones employed in this study. In this perspective, we preliminarily checked the capability to establish interfaces between polymer NPs and *A. thaliana* seedlings roots. The latter represent an excellent system to study plant responses to mechanical wounding and stress conditions.[80] SEM images show that P3HT NPs are well-adherent to the surface of roots (Figure S2, Supporting Information). Confocal fluorescence images further demonstrate that polymer NPs tend to distribute in close proximity to the root tip region, an organ particularly sensitive to environmental stimuli and able to direct root growth (Figure S3, Supporting Information).[80] Though preliminary, these data support the possibility to establish a close, functional interface also between P3HT NPs and plant roots, within in vivo, physiologically relevant conditions.

3. Conclusions

The present work shows that a biohybrid, photoactive interface between a prototypical conjugated polymer and GCs is possible. Of note, administration of polymer NPs does not have, per se, effects of stomatal physiology, whereas their optical activation sizably affects the open state of stomata and spontaneous cytosolic Ca^{2+} oscillations of GCs. Spatio-temporally controllable effects of photoactive nanomaterials on Ca^{2+} homeostasis in GCs can provide a novel research tool for the understanding of the complex interplay between cytosolic Ca^{2+} oscillations and stomatal movements, the current object of intense investigation in plant physiology.

In perspective, this work supports the possibility to employ light-responsive organic materials to downregulate on demand the stomatal aperture, by using visible light and in a drug-free, touchless, and easily controllable way. When transferred to the field, this strategy may represent an innovative approach to optimize the exchange of gases and water loss of plants, and to improve the plant resilience toward environmental constraints, in line with United Nation's Sustainable Development Goals. However, the full exploitation of the proposed approach must rely on a strong, comprehensive effort to develop and optimize ad hoc environmentally sustainable nanomaterials, able to regulate stomatal movements in physiologically relevant conditions. The administration strategy of polymer beads, as well as their localization and functional efficiency over time, should be considered in detail. Regulatory and safety issues should guide, from the very beginning, the synthesis by design of novel tools available to plant biotechnologies. Though, we believe that plant photobionics holds a great potential impact and will play a key role in the agriculture 4.0 of the next future.

4. Experimental Section

Poly(3-Hexylthiophene-2,5-Diyl) Nanoparticles Preparation and Optoelectronic Characterization: P3HT NPs were prepared as previously described, by employing the reprecipitation method.[42] Briefly, a solution of region-regular P3HT (purity, 99.995%; molecular weight, Mn 54.000–75.000; used as received from Sigma-Aldrich without further purification steps) 20 g L^{-1} in tetrahydrofuran (Sigma Aldrich) was added drop-wise to ultrapure water under magnetic stirring. The colloidal dispersion obtained was subjected to dialysis against 2 L of water overnight, for removing the residual organic solvent. The rr-P3HT-based colloidal suspension was centrifuged for 10 min at different rates, from 2000 to 8000 rpm, separating every time the supernatant from the precipitate, obtaining a wide range of samples with different particle dimensions (from 100 to 600 nm) and different optical density. The average hydrodynamic radius of the NPs and the solutions OD were characterized by carrying out dynamic light scattering measurements and using a TECAN Spark 10M Plate reader, respectively. P3HT NPs dispersions administered to the GCs cultures had an average hydrodynamic radius 237 ± 82 nm and a polydispersity index of 0.12. Optical absorbance was measured by UV–vis spectrophotometer (PERKIN-ELMER Lambda 1050 UV/Vis/NIR Spectrophotometer). SEM images were acquired by using a TESCAN microscope MIRA3. Prior to SEM image acquisition (operating voltage 4.5 kV), a P3HT NPs dispersion was drop-casted on top of a silver foil adhesive tape. The sample was then air-dried and covered by a thin gold layer (thickness 4 nm + 2 nm Cr adhesion layer) using a metal evaporator. Photoelectrochemical measurements were acquired using a potentiostat/galvanostat (Autolab, PGSTAT 302N) in a three-electrode configuration, divided into two compartments connected by a saline bridge. One compartment contained the ITO (XynYan Technology, 15 nm thickness, sheet resistance 15 Ohm sq^{-1}) working electrode and the P3HT NPs dissolved in the electrolyte solution (phosphate buffer 10 mM, pH 7). In the second compartment, the reference and the counter electrodes, a saturated KCl Ag/AgCl and Pt wire, respectively, were immersed in the pure electrolyte. A continuous light source (Thorlabs LED M470L3-C5, 470 nm central emission wavelength) was used for the photoexcitation (power density of 2.7 mW mm^{-2}).

Plant Material and Growth Conditions: *A. thaliana* plants were of the ecotype Columbia 0 (Col-0). Seeds were surface-sterilized by vapor-phase sterilization[81] and plated on half-strength MS medium (Murashige and Skoog, 1962)[82] (Duchefa, http://www.duchefa-biochemie.com/) supplemented with 0.1% sucrose, 0.05% MES, adjusted with TRIS-Base, and 0.8% plant agar (Duchefa, http://www.duchefa-biochemie.com/). After stratification at 4 °C in the dark for 2 days, plates were transferred to the growth chamber under long day conditions (16 h light/8 h dark, 100 µE m^{-2} s^{-1} of Cool White Neon lamps) at 22 °C. The plates were kept vertically, and seedlings were used for imaging 6–7 days after germination.

Arabidopsis plants were grown in soil under long day conditions (16 h light/8 h dark, 100 µE m^{-2} s^{-1} of Cool White Neon lamps) at 22 °C and 75% relative humidity were used.

Isolation of Guard Cells by Epidermal Strip Procedure: For GCs imaging the protocol reported in Behera and Kudla (2013) was followed.[46] Briefly, 6-week-old *A. thaliana* leaves were attached to microscope cover glasses (0.17 µm thickness) using a Medical adhesive (Hollister 7730, https://www.hollister.com/) and by gently pressing them with a paintbrush. Upper cells were removed by using a razor blade, thus leaving exposed a thin layer of GCs. The cells were then rapidly immersed in the imaging solution (5 mM KCl, 10 mM MES, 50 µM Ca^{2+}, pH 6.15 adjusted with TRIS-base), to quickly establish a physiological environment and to minimize stress conditions.

Guard Cells Viability: In viability assays GCs cultures were incubated with FDA (4 µg mL^{-1} in imaging solution) for 20 min. Then, bright field and fluorescence images of the FDA-stained GCs were acquired with an inverted fluorescence microscope (Nikon Ti-E) using a 20× objective (NA 0.75) and standard FITC filter set. Samples were then exposed to the P3HT polymer, and both P3HT-treated and untreated leaves were photoexcited with green light focalized by the microscope objective (λ = 540 nm, light intensity on the sample: 64 mW mm^{-2}) for 2 min. The acquisition of bright field and fluorescence images of the FDA-stained GCs was then repeated. The statistical analysis was done by manually counting the number of GCs for each field of view. The percentage of healthy cells was obtained as the ratio between the FDA-stained cells and the total number of cells counted in bright field images. 50 cells belonging to three statistically independent samples for each condition were considered for the statistical analysis.

Stomatal Opening Analysis: The authors employed *A. thaliana* leaves expressing the NES YC3.6 sensor. Epidermal strip procedure was the same as described above. GCs were treated with P3HT NPs (OD 0.1) or SiO_2 NPs, dispersed in the imaging solution. The latter was used as negative controls, had an average hydrodynamic radius of 260 ± 10 nm, and a concentration of 250 µg mL^{-1}. GCs were exposed to white light (4000 lux) for 90 min in a controlled environment. The measurement of the stomatal opening was carried out by fluorescence imaging (Nikon Ti-E inverted microscope), using a CFI Plan Apo Lambda 60X Oil (N.A. 1.4) and standard FITC filter sets. The stomatal aperture size was quantified using ImageJ software (https://imagej.nih.gov/ij/index.html). The measurement of the size of the stomata aperture was performed by two different investigators in double-blinded conditions. Mean values had been averaged over $n = 4$ statistically independent replicas; $n = 50$ cells for each condition.

Calcium Imaging Experiments: For Ca^{2+} imaging experiments the authors used *A. thaliana* plants expressing the NES YC3.6 sensor. Epidermal strip procedure was the same as described above. Imaging solution had the following composition: 5 mM KCl, 10 mM MES, 50 µM Ca^{2+}, pH 6.15 adjusted with TRIS-base. For treated samples, P3HT NPs (OD 0.1) were incubated with the imaging solution for 20 min. Ca^{2+} imaging analysis of the spontaneous GCs activity was carried out with an inverted fluorescence microscope (Nikon Ti-E) using a 20× objective (NA 0.75). The YC probe excitation was provided by a fluorescent lamp (Prior Lumen 200 PRO; Prior Scientific) with emission peak at 440 nm (436/20 nm). Images were acquired every 5 s with a Hamamatsu Dual CCD camera (ORCA-D2) using a FRET CFP/YFP optical block A11400-03 (emission 1, 483/32 nm for CFP; emission 2, 542/27 nm for FRET) with a dichroic 510 nm mirror (Hamamatsu) for the simultaneous CFP and YFP acquisitions. The exposure time was set to 100 ms and the CCD binning was 4 × 4. P3HT NPs' photoexcitation was provided by green light (emission peak, λ = 540 nm; photoexcitation density, 64 mW mm^{-2}; stimuli duration, 2 min). Statistical analysis was performed by considering $n = 10$ GCs for each condition, belonging to three statistically independent samples.

The experiments for the evaluation of the reversibility of the rr-P3HT NPs-induced effect were performed by repeating the calcium imaging experiments after leaving the GC samples resting in dark for 20 min.

Confocal Laser Scanning Microscopy: Confocal microscopy analyses of *Arabidopsis* GCs were performed using a Nikon Ti2 inverted microscope, equipped with a Nikon A1R+ laser scanning device (http://www.nikon.com/). Images were acquired by a Plan Apo λ 60x Oil objective. Cameleon YC3.6 was excited with the 488 nm laser and the emission was collected at 505–550 nm. P3HT NPs were excited with the 561 nm laser and the emission was collected at 570–620 nm. NIS-Elements (Nikon; http://www.nis-elements.com/) was used as a platform to control the microscope. Images were analyzed using NIS-Elements and FIJI.

Supporting Information

Supporting Information is available from the Wiley Online Library or from the author.

Acknowledgements

The authors gratefully acknowledge help from Dr. A. Desii in SEM images acquisition. M.R.A. and F.G. acknowledge support by the European Research Council (ERC) under the European Union's Horizon 2020 research and innovation program "LINCE", grant agreement no. 803621. A.C. acknowledges support by University of Milan, Piano di Sviluppo di

Ateneo 2019. Part of the imaging analyses were carried out at NOLIMITS, an advanced imaging facility established by the University of Milan.

Conflict of Interest

The authors declare no conflict of interest.

Author Contributions

M.R.A. and A.C. planned and supervised the work. G.T. fabricated and characterized NPs dispersions. A.C. provided *Arabidopsis thaliana* plant models and carried out epidermal strips. G.T., A.C., and M.R.A. performed viability and fluorescence imaging experiments. G.T. analyzed the data, with help from F.G, with a double-blinded approach. All authors interpreted the data. M.R.A. and G.T. wrote the main manuscript, with help from all authors.

Data Availability Statement

Research data are available from the corresponding authors on reasonable request.

Keywords

Arabidopsis thaliana, conjugated polymer nanoparticles, guard cells, organic bioelectronics, visible light

Received: February 12, 2021
Revised: April 16, 2021
Published online: May 13, 2021

[1] P. H. Raven, *Biology of Plants*, W. H. Freeman And Co., New York **2005**.
[2] T. T. S. Lew, V. B. Koman, P. Gordiichuk, M. Park, M. S. Strano, *Adv. Mater. Technol.* **2020**, *5*, 1900657.
[3] P. Cataldi, J. A. Heredia-Guerrero, S. Guzman-Puyol, L. Ceseracciu, L. L. Notte, A. Reale, J. Ren, Y. Zhang, L. Liu, M. Miscuglio, P. Savi, S. Piazza, M. Duocastella, G. Perotto, A. Athanassiou, I. S. Bayer, *Adv. Sustainable Syst.* **2018**, *2*, 1800069.
[4] Y. Wang, S. Li, L. Liu, F. Lv, S. Wang, *Angew. Chem., Int. Ed.* **2017**, *56*, 5308.
[5] J. Zhao, W. Ren, Y. Dai, L. Liu, Z. Wang, X. Yu, J. Zhang, X. Wang, B. Xing, *Environ. Sci. Technol.* **2017**, *51*, 7686.
[6] J. P. Giraldo, M. P. Landry, S. M. Faltermeier, T. P. McNicholas, N. M. Iverson, A. A. Boghossian, N. F. Reuel, A. J. Hilmer, F. Sen, J. A. Brew, M. S. Strano, *Nat. Mater.* **2014**, *13*, 400.
[7] Y. Li, X. Xu, Y. Wu, J. Zhuang, X. Zhang, H. Zhang, B. Lei, C. Hu, Y. Liu, *Mater. Chem. Front.* **2020**, *4*, 437.
[8] J. J. Richardson, K. Liang, *Small* **2018**, *14*, 1702958.
[9] Z. Guo, J. J. Richardson, B. Kong, K. Liang, *Sci. Adv.* **2020**, *6*, eaaz0330.
[10] X. Zhou, Y. Zeng, Y. Tang, Y. Huang, F. Lv, L. Liu, S. Wang, *Sci. Adv.* **2020**, *6*, eabc5237.
[11] E. Stavrinidou, R. Gabrielsson, E. Gomez, X. Crispin, O. Nilsson, D. T. Simon, M. Berggren, *Sci. Adv.* **2015**, *1*, e1501136.
[12] E. Stavrinidou, R. Gabrielsson, K. P. R. Nilsson, S. K. Singh, J. F. Franco-Gonzalez, A. V. Volkov, M. P. Jonsson, A. Grimoldi, M. Elgland, I. V. Zozoulenko, D. T. Simon, M. Berggren, *Proc. Natl. Acad. Sci. USA* **2017**, *114*, 2807.
[13] G. Dufil, D. Parker, J. Y. Gerasimov, T.-Q. Nguyen, M. Berggren, E. Stavrinidou, *J. Mater. Chem. B* **2020**, *8*, 4221.
[14] N. Coppedè, M. Janni, M. Bettelli, C. L. Maida, F. Gentile, M. Villani, R. Ruotolo, S. Iannotta, N. Marmiroli, M. Marmiroli, A. Zappettini, *Sci. Rep.* **2017**, *7*, 16165.
[15] F. Vurro, M. Janni, N. Coppedè, F. Gentile, R. Manfredi, M. Bettelli, A. Zappettini, *Sensors* **2019**, *19*, 4667.
[16] H. Yuan, Y. Fan, C. Xing, R. Niu, R. Chai, Y. Zhan, J. Qi, H. An, J. Xu, *Anal. Chem.* **2016**, *88*, 6593.
[17] D. W. Meinke, *Science* **1998**, *282*, 662.
[18] T. Mitchell-Olds, *Trends in Ecol. Evol.* **2001**, *16*, 693.
[19] E. Zeiger, *Annu. Rev. Plant Physiol.* **1983**, *34*, 441.
[20] M. Krebs, K. Held, A. Binder, K. Hashimoto, G. D. Herder, M. Parniske, J. Kudla, K. Schumacher, *Plant J.* **2012**, *69*, 181.
[21] A. A. R. Webb, M. R. McAinsh, J. E. Taylor, A. M. Hetherington, J. A. Callow, in *Advances in Botanical Research*, Elsevier, Amsterdam **1996**, pp. 45–96.
[22] J. Kudla, D. Becker, E. Grill, R. Hedrich, M. Hippler, U. Kummer, M. Parniske, T. Romeis, K. Schumacher, *New Phytol.* **2018**, *218*, 414.
[23] A. Costa, L. Navazio, I. Szabo, *J. Exp. Bot.* **2018**, *69*, 4175.
[24] A. N. Dodd, J. Kudla, D. Sanders, *Annu. Rev. Plant Biol.* **2010**, *61*, 593.
[25] J. I. Schroeder, G. J. Allen, V. Hugouvieux, J. M. Kwak, D. Waner, *Annu. Rev. Plant Physiol. Plant Mol. Biol.* **2001**, *52*, 627.
[26] T.-H. Kim, M. Böhmer, H. Hu, N. Nishimura, J. I. Schroeder, *Annu. Rev. Plant Biol.* **2010**, *61*, 561.
[27] G. Tullii, F. Giona, F. Lodola, S. Bonfadini, C. Bossio, S. Varo, A. Desii, L. Criante, C. Sala, M. Pasini, C. Verpelli, F. Galeotti, M. R. Antognazza, *ACS Appl. Mater. Interfaces* **2019**, *11*, 28125.
[28] G. Tullii, A. Desii, C. Bossio, S. Bellani, M. Colombo, N. Martino, M. R. Antognazza, G. Lanzani, *Org. Electron.* **2017**, *46*, 88.
[29] C. Bossio, I. A. Aziz, G. Tullii, E. Zucchetti, D. Debellis, M. Zangoli, F. Di Maria, G. Lanzani, M. R. Antognazza, *Front. Bioeng. Biotechnol.* **2018**, *6*, 114.
[30] F. Lodola, V. Rosti, G. Tullii, A. Desii, L. Tapella, P. Catarsi, D. Lim, F. Moccia, M. R. Antognazza, *Sci. Adv.* **2019**, *5*, eaav4620.
[31] J. F. Maya-Vetencourt, D. Ghezzi, M. R. Antognazza, E. Colombo, M. Mete, P. Feyen, A. Desii, A. Buschiazzo, M. Di Paolo, S. Di Marco, F. Ticconi, L. Emionite, D. Shmal, C. Marini, I. Donelli, G. Freddi, R. Maccarone, S. Bisti, G. Sambuceti, G. Pertile, G. Lanzani, F. Benfenati, *Nat. Mater.* **2017**, *16*, 681.
[32] V. Benfenati, N. Martino, M. R. Antognazza, A. Pistone, S. Toffanin, S. Ferroni, G. Lanzani, M. Muccini, *Adv. Healthcare Mater.* **2014**, *3*, 392.
[33] O. S. Abdullaeva, M. Schulz, F. Balzer, J. Parisi, A. Lützen, K. Dedek, M. Schiek, *Langmuir* **2016**, *32*, 8533.
[34] M. L. DiFrancesco, E. Colombo, E. D. Papaleo, J. F. Maya-Vetencourt, G. Manfredi, G. Lanzani, F. Benfenati, *Carbon* **2020**, *162*, 308.
[35] K. Yang, J. Y. Oh, J. S. Lee, Y. Jin, G.-E. Chang, S. S. Chae, E. Cheong, H. K. Baik, S.-W. Cho, *Theranostics* **2017**, *7*, 4591.
[36] S. Vaquero, C. Bossio, S. Bellani, N. Martino, E. Zucchetti, G. Lanzani, M. R. Antognazza, *J. Mater. Chem. B* **2016**, *4*, 5272.
[37] M. R. Antognazza, M. Di Paolo, D. Ghezzi, M. Mete, S. Di Marco, J. F. Maya-Vetencourt, R. Maccarone, A. Desii, F. Di Fonzo, M. Bramini, A. Russo, L. Laudato, I. Donelli, M. Cilli, G. Freddi, G. Pertile, G. Lanzani, S. Bisti, F. Benfenati, *Adv. Healthcare Mater.* **2016**, *5*, 2271.
[38] E. Mosconi, P. Salvatori, M. I. Saba, A. Mattoni, S. Bellani, F. Bruni, B. S. Gonzalez, M. R. Antognazza, S. Brovelli, G. Lanzani, H. Li, J.-L. Brédas, F. De Angelis, *ACS Energy Lett.* **2016**, *1*, 454.
[39] R. Porrazzo, A. Luzio, S. Bellani, G. E. Bonacchini, Y.-Y. Noh, Y.-H. Kim, G. Lanzani, M. R. Antognazza, M. Caironi, *ACS Omega* **2017**, *2*, 1.

[40] D. Ghezzi, M. R. Antognazza, R. Maccarone, S. Bellani, E. Lanzarini, N. Martino, M. Mete, G. Pertile, S. Bisti, G. Lanzani, F. Benfenati, *Nat. Photon.* **2013**, *7*, 400.
[41] P. Feyen, E. Colombo, D. Endeman, M. Nova, L. Laudato, N. Martino, M. R. Antognazza, G. Lanzani, F. Benfenati, D. Ghezzi, *Sci. Rep.* **2016**, *6*, 22718.
[42] E. Zucchetti, M. Zangoli, I. Bargigia, C. Bossio, F. Di Maria, G. Barbarella, C. D'Andrea, G. Lanzani, M. R. Antognazza, *J. Mater. Chem. B* **2017**, *5*, 565.
[43] F. Di Maria, F. Lodola, E. Zucchetti, F. Benfenati, G. Lanzani, *Chem. Soc. Rev.* **2018**, *47*, 4757.
[44] J. F. Maya-Vetencourt, G. Manfredi, M. Mete, E. Colombo, M. Bramini, S. Di Marco, D. Shmal, G. Mantero, M. Dipalo, A. Rocchi, M. L. DiFrancesco, E. D. Papaleo, A. Russo, J. Barsotti, C. Eleftheriou, F. Di Maria, V. Cossu, F. Piazza, L. Emionite, F. Ticconi, C. Marini, G. Sambuceti, G. Pertile, G. Lanzani, F. Benfenati, *Nat. Nanotechnol.* **2020**, *15*, 698.
[45] J. M. Christie, M. D. Zurbriggen, *New Phytol.* **2020**, *229*, 3108.
[46] S. Behera, J. Kudla, *Cold Spring Harbor Protoc.* **2013**, *2013*, pdb. prot072983.
[47] J. M. Widholm, *Stain Technol.* **1972**, *47*, 189.
[48] L. Jiajia, M. Shinghung, Z. Jiacheng, W. Jialing, X. Dilin, H. Shengquan, Z. Zaijun, W. Qinwen, H. Yifan, C. Wei, *J. Visualized Exp.* **2017**, *123*, e55442.
[49] P. Hu, J. An, M. M. Faulkner, H. Wu, Z. Li, X. Tian, J. P. Giraldo, *ACS Nano* **2020**, *14*, 7970.
[50] M. Faralli, J. Matthews, T. Lawson, *Curr. Opin. Plant Biol.* **2019**, *49*, 1.
[51] W. L. Araújo, A. R. Fernie, A. Nunes-Nesi, *Plant Signaling Behav.* **2011**, *6*, 1305.
[52] T. Lawson, M. R. Blatt, *Plant Physiol.* **2014**, *164*, 1556.
[53] Y. Murata, I. C. Mori, S. Munemasa, *Annu. Rev. Plant Biol.* **2015**, *66*, 369.
[54] R. J. Jones, T. A. Mansfield, *J. Exp. Bot.* **1970**, *21*, 714.
[55] C. Garcia-Mata, L. Lamattina, *Nitric Oxide* **2007**, *17*, 143.
[56] T. Furuichi, H. Tatsumi, M. Sokabe, *Biochem. Biophys. Res. Commun.* **2008**, *366*, 758.
[57] S. Agurla, S. Gahir, S. Munemasa, Y. Murata, A. S. Raghavendra, in *Survival Strategies in Extreme Cold and Desiccation*, (Eds: M. Iwaya-Inoue, M. Sakurai, M. Uemura), Springer Singapore, Singapore **2018**, pp. 215–232.
[58] J. Yan, N. Tsuichihara, T. Etoh, S. Iwai, *Plant, Cell Environ.* **2007**, *30*, 1320.
[59] G. J. Allen, K. Kuchitsu, S. P. Chu, Y. Murata, J. I. Schroeder, *Plant Cell* **1999**, *11*, 1785.
[60] G. E. Gudesblat, N. D. Iusem, P. C. Morris, *New Phytol.* **2007**, *173*, 713.
[61] W.-H. Wang, X.-Q. Yi, A.-D. Han, T.-W. Liu, J. Chen, F.-H. Wu, X.-J. Dong, J.-X. He, Z.-M. Pei, H.-L. Zheng, *J. Exp. Bot.* **2012**, *63*, 177.
[62] F. Van Breusegem, E. Vranová, J. F. Dat, D. Inzé, *Plant Sci.* **2001**, *161*, 405.
[63] R. Singh, P. Parihar, S. Singh, R. K. Mishra, V. P. Singh, S. M. Prasad, *Redox Biol.* **2017**, *11*, 213.
[64] B. Halliwell, *Plant Physiol.* **2006**, *141*, 312.
[65] I. A. Aziz, M. Malferrari, F. Roggiani, G. Tullii, S. Rapino, M. R. Antognazza, *iScience* **2020**, *23*, 101091.
[66] C. Minguet-Parramona, Y. Wang, A. Hills, S. Vialet-Chabrand, H. Griffiths, S. Rogers, T. Lawson, V. L. Lew, M. R. Blatt, *Plant Physiol.* **2016**, *170*, 33.
[67] G. Loro, S. Wagner, F. G. Doccula, S. Behera, S. Weinl, J. Kudla, M. Schwarzländer, A. Costa, M. Zottini, *Plant Physiol.* **2016**, *171*, 2317.
[68] K. De Vriese, A. Costa, T. Beeckman, S. Vanneste, *Int. J. Mol. Sci.* **2018**, *19*, 1506.
[69] S. Behera, M. Krebs, G. Loro, K. Schumacher, A. Costa, J. Kudla, *Cold Spring Harbor Protoc.* **2013**, pdb.top066183.
[70] Y. Yang, A. Costa, N. Leonhardt, R. S. Siegel, J. I. Schroeder, *Plant Methods* **2008**, *4*, 6.
[71] M. R. McAinsh, A. A. R. Webb, J. E. Taylor, *Plant Cell* **1995**, *7*, 1207.
[72] G. J. Allen, J. M. Kwak, S. P. Chu, J. Llopis, R. Y. Tsien, J. F. Harper, J. I. Schroeder, *Plant J.* **1999**, *19*, 735.
[73] K. E. Hubbard, R. S. Siegel, G. Valerio, B. Brandt, J. I. Schroeder, *Ann. Bot.* **2012**, *109*, 5.
[74] M. Klejchova, F. A. L. Silva-Alvim, M. R. Blatt, J. C. Alvim, *Plant Physiol.* **2021**, *185*, 1523.
[75] P. S. Shacklock, N. D. Read, A. J. Trewavas, *Nature* **1992**, *358*, 753.
[76] I. D. Volotovski, S. G. Sokolovsky, E. L. Nikiforov, V. P. Zinchenko, *J. Photochem. Photobiol., B* **1993**, *20*, 95.
[77] W. R. Briggs, J. M. Christie, *Trends Plant Sci.* **2002**, *7*, 204.
[78] X. Zhao, Y.-L. Wang, X.-R. Qiao, J. Wang, L.-D. Wang, C.-S. Xu, X. Zhang, *Plant Physiol.* **2013**, *162*, 1539.
[79] G. J. Allen, S. P. Chu, C. L. Harrington, K. Schumacher, T. Hoffmann, Y. Y. Tang, E. Grill, J. I. Schroeder, *Nature* **2001**, *411*, 1053.
[80] J. M. Fasano, G. D. Massa, S. Gilroy, *J. Plant Growth Regul.* **2002**, *21*, 71.
[81] S. J. Clough, A. F. Bent, *Plant J.* **1998**, *16*, 735.
[82] T. Murashige, F. Skoog, *Physiol. Plant.* **1962**, *15*, 473.